Theoretical Study of the Effect of the Intermolecular Spin−Orbit Interaction in the Collision-Induced Intersystem Crossing of S_1 State Glyoxal by Ar

Tohru Nakajima*,† and Shigeki Kato‡

Department of Chemical System Engineering, Graduate School of Engineering, University of Tokyo, Tokyo 113-8656, Japan, and Department of Chemistry, Graduate School of Science, Kyoto University, Kyoto 606-8502, Japan

Received: August 1, 2001; In Final Form: September 14, 2001

The intersystem crossing from S_1 to T_1 in glyoxal induced by the collision of Ar has been studied theoretically. In particular, we have focused on the effects of the intermolecular spin−orbit interaction, which was not considered important in this process. The interaction potential of S_1 in the glyoxal and Ar system was carried out by the CASSCF method. Further, the interaction potential of T_1 and the spin−orbit interaction, which is represented by the Breit-Pauli Hamiltonian, between S_1 and T_1 were calculated by the full-CI method with the same active spaces and molecular orbitals as those of the CASSCF calculations for S_1. Using these calculation results, the semiclassical dynamics calculations were employed to estimate the transition cross sections and rate constants. It is found that the intermolecular spin−orbit interaction largely amplifies the transition probabilities and the relaxation on the T_1 state is indispensable to describing the dynamics in this intersystem crossing.

1. Introduction

Collision-induced intersystem crossing of polyatomic molecules has long been studied experimentally.[1−3] Glyoxal is one of the prototype molecules in these studies. It has been established that the intersystem crossing in glyoxal from the S_1 state to T_1 can easily occur under the existence of perturbers such as hydrogen molecules and helium or argon atoms, although it rarely occurs in an isolated condition.

Freed et al. studied the collision-induced intersystem crossing theoretically in the 1970s.[4] They proposed that the intersystem crossing is mediated by the mixing of the vibronic states of S_1 manifold with those of T_1, which is caused by the intramolecular spin−orbit (SO) interaction in glyoxal, and is amplified by the vibrational and rotational relaxations within the T_1 vibronic states in the course of the collision with the perturber as the principal reaction mechanism. The intermolecular SO interaction between glyoxal and perturber was not considered to be an important factor on the basis of the experimental results by Beyer, Zittel, and Lineberger[1] showing that the cross section of the collision-induced intersystem crossing does not depend on the atomic numbers of perturbers.

Recently, Dai, and co-workers[5] suggested that the intermolecular SO interaction affects the lifetime of the initially prepared vibronic states of S_1 in glyoxal from their experimental results using the three different isomers of van der Waals complexes consisting of glyoxal and Ar. From the theoretical study, Hoffmann and Schatz[6] discussed the importance of orientation dependence of the intermolecular SO interaction in the intersystem crossing of the $O + H_2$ reaction. It seems natural to consider that there also exist some effects of the intermolecular SO interaction on the collision-induced intersystem crossing.

Our purpose in the present paper is to carry out theoretical calculations in order to examine the importance of the intermolecular SO interaction in the intersystem crossing process from the S_1 state glyoxal to T_1 induced by the collision with Ar. We performed ab initio molecular orbital (MO) calculations of the interaction energies between Ar and glyoxal in the S_1 and T_1 states and the matrix elements of the intra and intermolecular SO interactions between the S_1 and T_1 states. Dynamics calculations based on a semiclassical method were also carried out to obtain the transition probabilities and total cross sections. To our knowledge, theoretical studies of the collision-induced intersystem crossing based on ab initio calculations of the interaction potentials and SO coupling elements are virtually nonexistent. In section 2, calculation methods for electronic states and dynamics employed here are described. In section 3, we show the results of calculations and discuss the importance of the intermolecular SO interaction on the intersystem crossing. The concluding remarks are summarized in section 4.

2. Calculation Methods

A. Potential Energy Surface. Throughout this work, we used the Gaussian basis sets of double-ζ plus polarization quality (DZP). For the constituent atoms of glyoxal, the Huzinage−Dunning−Raffenetti [9s5p1d/3s2p1d]/(3s1p/2s1p) basis set[7] has been employed. For Ar atom, the [12s8p/5s3p] basis set[8] by Mclean and Chandler with a set of d polarization functions ($\zeta = 0.696$) was used.

First, we performed the geometry optimizations of glyoxal in the S_0, S_1, and T_1 states in the C_{2h} symmetry.[9] Using the analytical method for the second derivatives of the energy,[10] the normal-mode analyses were done at each the equilibrium

* Corresponding author.
† University of Tokyo.
‡ Kyoto University.

10.1021/jp012970u CCC: $20.00
Published on Web 11/03/2001

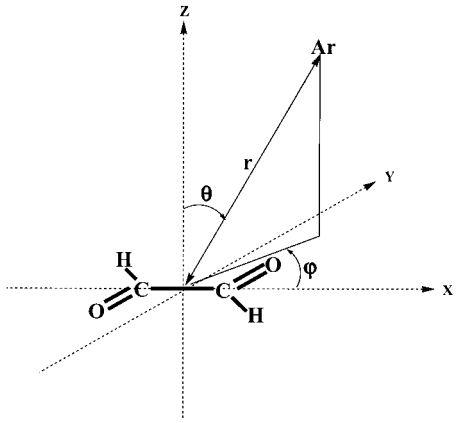

Figure 1. Spherical polar coordinates, which are described in terms of radius r, zenithal θ ($0.0° < \theta < 180.0°$), and azimuth φ ($-180.0° < \varphi < 180.0°$), are used. The origin is the center of mass of glyoxal. Glyoxal is a planar molecule in the S_0, S_1, and T_1 states and lies on the plane defined by $\theta = 90.0°$. The axis of the carbon−carbon bond corresponds to that of $\varphi = 0.0°$ and 180.0°, and two oxygen atoms are arranged in $0.0° < \varphi < 90.0°$ and $-180.0° < \varphi < -90.0°$, respectively. From the result of the geometry optimization for S_1, the positions of oxygen, hydrogen, and carbon atoms are $r = 1.756$ Å, $\theta = 90.0°$, $\varphi = 38.7°$ and $-141.3°$, $r = 1.561$ Å, $\theta = 90.0°$, $\varphi = -36.5°$ and 143.5°, and $r = 0.710$ Å, $\theta = 90.0°$, $\varphi = 0.0°$ and 180.0°, respectively.

structure to construct the vibrational basis sets of the S_1 and T_1 states, which were required in the calculations of Franck−Condon factors[11] and collision dynamics as described later. In these calculations, the eight-in-six (eight electrons in six orbitals) complete active space self-consistent field (CASSCF) wave functions were used. We also carried out the multireference configuration interaction (MRCI) calculations[12] to obtain estimates that are more reliable for the energy differences between these electronic states. The MRCI energies were further improved by adding the energy correction terms by Davidson or Pople.[13]

Next, we calculated the interaction energies between Ar and glyoxal in the S_1 state by the eight-in-six CASSCF method. Using the one-electron orbitals for S_1, we further carried out full-CI calculations[14] within the same active space as that of the CASSCF calculations to obtain the T_1 state interaction energies. It is noted that the results for S_1 by the full-CI calculations are identical as those by the eight-in-six CASSCF. The resultant CI wave functions for S_1 and T_1 were used in the SO interaction calculations. The coordinate system for describing the glyoxal and Ar system is shown in Figure 1, where the geometry of glyoxal was fixed at the optimized geometry of S_1 in an isolated state since we make an issue of the region where the interaction energy is sufficiently low. Calculations were performed about 150 points with respect to a quarter of the sphere under the consideration of the symmetry of glyoxal (for r, every 0.5 Å from ~3.0 to 6.0 Å; for θ, every 30° from 0° to 90°, and for φ, every 30° from −90° to 90°).

Finally, we represented the interaction potentials for both the S_1 and T_1 states by the following analytic function:[15]

$$A \exp\{-B(r - r_1)\} - C(r - r_2)^{-6} \tag{1}$$

where the parameters A, B, C, r_1, and r_2 are determined by the least-squares fitting procedure as the function of orientation angles θ and φ.

B. Spin−Orbit Interaction. We calculated the matrix elements of the SO interaction between the S_1 and T_1 states using the full-CI wave functions described above. The Breit-Pauli SO Hamiltonian ($\hat{H}_{SO}$)[16,17]

$$\hat{H}_{SO} = \frac{e^2\hbar}{2m^2c^2}\left\{\sum_k\sum_\alpha \frac{Z_\alpha}{r_{\alpha k}^3}[(\vec{r}_k - \vec{r}_a) \times \vec{p}_k]\cdot\vec{s}(k) - \sum_{k,j\neq k}\frac{1}{r_{kj}^3}[(\vec{r}_k - \vec{r}_j) \times \vec{p}_k]\cdot[\vec{s}(k) + 2\vec{s}(j)]\right\} \tag{2}$$

which includes both the one- and two-electron contributions. For the intermolecular term, the matrix elements were calculated at all the 150 points as for the interaction energy. The resultant matrix elements were fitted to the analytical function[15]

$$A \exp[-B(r - r_0)] \tag{3}$$

Here, A, B, and r_0 are the parameters given as the functions of θ and φ.

C. Dynamics Calculations. Semiclassical dynamics calculations[18] were carried out to evaluate the cross sections of the transition from S_1 to T_1 in glyoxal affected by the collision with Ar. In these calculations, we constructed the vibronic basis functions by the direct product of the electronic wave functions of glyoxal + Ar and the vibrational wave functions of glyoxal obtained from the normal-mode analyses. We adopted the infinite-order sudden (IOS) approximation[19] to avoid taking the rotational wave functions into account explicitly.

The dynamics calculations are based on the equation of time-dependent probability amplitudes ($a_n(t)$), which is expressed in the following:[18]

$$i\hbar\frac{da_n(t)}{dt} = \sum_m V_{nm}\exp(i\omega_{nm}t)a_m(t) \tag{4}$$

where

$$\omega_{nm} = \frac{(E_n - E_m)}{\hbar} \tag{5}$$

and

$$V_{nm} = \langle\phi_n(\rho)|\hat{V}(r(t),\rho)|\phi_m(\rho)\rangle \tag{6}$$

Here, ρ denotes the set of internal coordinates of glyoxal, and $r(t)$ is the distance between the center of the mass of glyoxal and Ar at time t. $\phi_n(\rho)$ and E_n are the n-th vibronic wave function of glyoxal and its energy, respectively. $\hat{V}(r(t),\rho)$ represents the interaction potential and the SO interaction. V_{nm}'s are specifically given as follows:

$$\langle\psi_S\chi^S_{\{\nu\}}|\hat{V}(r(t),\rho)|\psi_S\chi^S_{\{\nu'\}}\rangle = \langle\psi_S|\hat{V}|\psi_S\rangle\delta_{\{\nu\}\{\nu'\}} = V_S\delta_{\{\nu\}\{\nu'\}}(n,m\in S_1) \tag{7-a}$$

$$\langle\psi_T\chi^T_{\{\nu\}}|\hat{V}(r(t),\rho)|\psi_T\chi^T_{\{\nu'\}}\rangle = \langle\psi_T|\hat{V}|\psi_T\rangle\delta_{\{\nu\}\{\nu'\}}\delta_{m_Tm_T} = V_T\delta_{\{\nu\}\{\nu'\}}\delta_{m_Tm_T}(n,m\in T_1) \tag{7-b}$$

$$\langle\psi_S\chi^S_{\{\nu\}}|\hat{V}(r(t),\rho)|\psi_T\chi^T_{\{\nu'\}}\rangle = \langle\psi_S|\hat{H}_{SO}|\psi_T\rangle F_{\{\nu\}\{\nu'\}} = V_{ST}F_{\{\nu\}\{\nu'\}}(n\in S_1,m\in T_1) \tag{7-c}$$

Here, $\phi_n = \psi_n\chi^n$, with ψ_n and χ^n being the electronic and vibrational wave functions, respectively. m_T is the spin magnetic quantum number of T_1. $F_{\{\nu\}\{\nu'\}}$ is the Franck−Condon factor between the vibrational states $\{\nu\}$ and $\{\nu'\}$, which belong to

the S_1 and T_1 manifold, respectively. V_{ST} represents the SO interaction matrix element between the different electronic states. V_S and V_T are the interaction potentials of S_1 and T_1, respectively. We used the analytic functions (eqs 1 and 3) for V_S, V_T, and V_{ST} as described above.

Under the IOS approximation, we carried out calculations in the 19 fixed orientations of Ar with respect to glyoxal (every 30° with respect to θ and φ) to cover the quarter of the sphere. The relative translational energy was chosen to be 69.50 cm^{-1}(100.0 K) and 207.22 cm^{-1}(298.15 K), and the range of orbital angular momentum quantum number (l) was 0−150. The initial condition for the probability amplitudes was

$$a_n(-\infty) = \delta_{ng} \tag{8}$$

and the vibronic states were evolved in time. Here, g stands the vibrational ground state of S_1, which was supposed to be the initial state.

Since the transition probabilities are sufficiently small, we adopted the perturbation theory[18] in the dynamics calculation. Equation 4 is thus transformed into the expression

$$a_n(t) = \frac{1}{i\hbar}\int_{t_0}^{t} V_{ng}(r(\tau)) \exp(i\omega_{ng}\tau) a_g(t_0)\, d\tau \tag{9}$$

where the subscripts n stands for the n-th vibrational state of T_1. t_0 means the starting time of the density transition from S_1 to T_1 affected by the collision with Ar. Hereafter, the dynamics calculation described above is denoted as method 1.

In the actual collision-induced intersystem crossing, the vibrational−rotational relaxation on the vibronic states of T_1 plays an important role to induce the irreversible electronic transition from S_1 to T_1. Therefore, the transition probabilities and the total cross sections obtained by method 1 become too small in comparison with those of the experiments. To take account of the relaxation effect,[4] we introduced the following effective Hamiltonian ($\hat{H}_{eff}$):[20]

$$\hat{H}_{eff} = \hat{H} - \frac{i\Gamma_n}{2} \tag{10}$$

where Γ_n is the level width of the n-th vibrational state of T_1. The time evolution of the probability amplitude ($a_g(t)$) is given by

$$\frac{da_g(t)}{dt} = -\frac{1}{\hbar^2}\sum_n V_{gn} \exp(i\omega_{gn}t) \exp\left(-\frac{\Gamma_n t}{2\hbar}\right)\int_{t_0}^{t} V_{ng} \exp(-i\omega_{gn}\tau) \exp\left(\frac{\Gamma_n \tau}{2\hbar}\right) a_g(\tau)\, d\tau \tag{11}$$

The level widths are the parameters to control the strength of the relaxation effect in the T_1 state. We obtained the value of 0.8 cm^{-1} as the averaged energy level spacing among the vibrational states of T_1 in the vicinity of the vibrational ground state of S_1 from the Franck−Condon factor calculation. To simplify the calculations and to model a quasicontinuum of T_1 by lifetime broadening due to the collision-induced vibrational−rotational relaxations, all the values of Γ_n were set to be 1.0 cm^{-1}, the lifetime of 5.3 ps. Using the perturbation theory[18] again, eq 11 is also written in the form

$$a_n(t) = \frac{1}{i\hbar}\int_{t_0}^{t} V_{ng}(r(\tau)) \exp(i\omega_{ng}\tau) \exp\left(-\frac{\Gamma_n \tau}{2\hbar}\right) a_g(t_0)\, d\tau \tag{12}$$

Hereafter, the dynamics calculation using eq 12 is denoted as method 2.

TABLE 1: Geometry Parameters in S_0, S_1, and T_1 States of Glyoxal[a]

	S_0		S_1		T_1	
	cal.	expl.[b]	cal.	expl.[c]	cal.	expl.
r_{C-H}	1.088	1.132	1.077	1.115	1.076	−
r_{C-C}	1.508	1.526	1.419	1.460	1.435	−
r_{C-O}	1.208	1.212	1.281	1.252	1.265	−
∠CCH	116.2	112.2	121.1	114.0	120.9	−
∠CCO	121.1	121.2	120.4	123.7	119.8	−

[a] Å for bond lengths and deg for bond angles. [b] Taken from ref 22j. [c] Taken from ref 22i.

TABLE 2: Energy Difference between S_0, T_1, and S_1 States (kcal/mol)[a]

	CASSCF	MRCI	MRCI (Davidson)	MRCI (Pople)	expl.
$E(S_1) - E(S_0)$	79.79	74.05	70.49	70.07	62.8[b]
$E(T_1) - E(S_0)$	73.69	65.64	61.68	61.83	54.9[c]
$E(S_1) - E(T_1)$	6.10	8.41	8.82	8.24	7.9[b,c]

[a] Geometries are optimized by the eight-in-six CASSCF method. Zero-point energies by the CASSCF method are included. [b] Taken from ref 22h. [c] Taken from ref 22g.

3. Results and Discussion

The optimized geometric parameters of S_0, S_1, and T_1 are listed in Table 1. The discrepancy between the calculated and experimental geometries for the S_1 state may be attributed to the instability problem[21] i.e., the symmetry-broken solutions with a lower symmetry than the C_{2h} nuclear framework exist in the CASSCF wave functions for the excited states. It seems that the excited-state CASSCF wave function overemphasizes the O−C═C−O resonance structure. As seen in Table 1, the T_1 state optimized geometry is very close to that of S_1, indicating that the intersystem crossing from S_1 to T_1 hardly occurs due to small values of the Franck−Condon factors between the initial vibrational state of S_1 and the numerous isoenergitic vibrational states of T_1.

The calculated adiabatic energy differences including the zero-point energy corrections between S_0, S_1, and T_1 are given in Table 2. In the CASSCF method, the adiabatic excitation energies to the S_1 and T_1 states from S_0 are overestimated, while the S_1−T_1 difference is underestimated compared to the experiments. In the MRCI calculations, these energy differences are improved from the CASSCF values since the energy lowering of the S_1 and T_1 states due to the dynamical correlation effect is larger than that of S_0. The energy difference between S_1 and T_1 by MRCI with the Pople correction (8.24kcal/mol) is in excellent agreement with that by the experiments (7.9kcal/mol). We use the MRCI value with the Pople correction for the S_1−T_1energy difference in the following dynamics calculations.

The normal-mode frequencies at the optimized geometries of S_1 and T_1 by the eight-in-six CASSCF method are shown in Table 3 along with the experimental values. The calculated results agree with the experimental ones[22] in the low-frequency region. However, there are large differences between the calculated and experimental frequencies in the high-frequency region. The discrepancy with respect to the C═O stretching (b_u) mode should be remarked, which is also associated with the symmetry-breaking problem.[21] We calculated the Franck−Condon factors between the vibrational ground state of S_1 and the numerous vibrational states of T_1 by the method developed by Kupka and Cribb[11] for the use of dynamics calculations. The discrepancy in the C═O stretching (b_u) mode may affect the

TABLE 3: Vibrational Frequencies in S_1 and T_1 States of Glyoxal C_{2h} (cm^{-1})

mode	symmetry species	S_1 calc.	S_1 expl.[a]	T_1 calc.	T_1 expl.[b]
torsional	a_u	234	233	259	234
C−C═O bending	b_u	396	379	409	392
C−C═O bending	a_g	582	509	572	502
C−H wagging	b_g	745	735	740	700
C−H wagging	a_u	813	720	800	727
C−C stretching	a_g	1189	952	1179	961
C═O stretching	a_g	1297	1391	1360	1459
C−H rocking	b_u	1362	1172	1368	−
C−H rocking	a_g	1507	1195	1508	1195 (1415[c])
C═O stretching	b_u	2328	1281	2474	−
C−H stretching	a_g	3374	2809	3376	−
C−H stretching	b_u	3400	2835[b]	3422	−

[a] Taken from ref 22f. [b] Taken from ref 22g. [c] Taken from ref 22c.

Franck−Condon factors. However, the normal coordinate corresponding to this mode is largely localized to the C═O stretching coordinate, and the frequencies of other b_u modes are close to the experimental values.

The potential energy surface of S_1 in the glyoxal and Ar system is shown in Figure 2a−d. These figures are drawn in the geometric range $0.0° < \theta < 90.0°$ and $-90.0° < \varphi < 90.0°$ in consideration of the symmetry of glyoxal (see Figure 1). The positions of C, O, and H atoms are the same as those of the S_1 optimized geometry. In calculating the interaction potential, we used the first-order convergence procedure with the initial MO vectors constructed from the C_{2h} MO vectors of isolated glyoxal and Ar ones in order to avoid the symmetry-breaking problem.[21] We found that the glyoxal MOs obtained in the C_{2h} symmetry are well retained even for the glyoxal and Ar interacting system in the region of moderate interaction energy. The interaction potential is mainly dominated by the steric repulsion between glyoxal and Ar. As shown in Figure 2a ($\theta = 90.0°$), the potential energy surface is characterized by a strong repulsion between O and Ar and a relatively weak repulsion between H and Ar and shows a rather complicated shape. However, the shape of potential energy surface becomes simpler as θ decreases. At $\theta = 30.0°$ (Figure 2c), the potential energy surface feature is almost independent of angle φ.

Another important feature of the potential energy surface is the existence of shallow minimums in the neighborhood of $r = 4.5$ Å. It has been pointed out that glyoxal and Ar could be formed into the van der Waals complexes. Among three different isomers in the S_1 state deduced from the experiments and simulations by Dai and co-workers,[5] the minimum at $r = 4.7$ Å, $\theta = 90.0°$, and $\varphi = -30.0°$ in Figure 2a corresponds to the front isomer by Dai et al., though the position is slightly different from the experimental estimate, $r = 4.23$ Å, $\theta = 80.0°$, and $\varphi = -48.0°$. We also found very shallow wells corresponding to their top and side isomers. Our calculations further show that the existence of the potential minimums at $r = 4.5$ Å, $\theta = 30.0°$, $\varphi = 0.0°$ in Figure 2c and $r = 4.5$ Å, $\theta = \pm 60.0°$, $\varphi = \pm 90.0°$ in Figure 2d, which are not observed experimentally. It is noted that it is important to include the dynamical electron correlation effect to obtain the precise positions and well depths for van der Waals complexes. Despite the lack of dynamical electron correlation effect, the present interaction potential can be used in the dynamics calculations since the collision dynamics at room temperatures is mainly dictated by the repulsive part of potential. The analytical function, eq 1, reproduces the ab initio energies very well, within the error of 5 cm^{-1}.

The potential surface of T_1 in the glyoxal and Ar system has characteristics very similar to that of S_1. These potential surfaces are almost parallel each other and never cross in the weak interaction region, where the repulsion energies between glyoxal and Ar are up to 10kcal/mol in both the S_1 and T_1 states. The differences between these potential surfaces are in the range

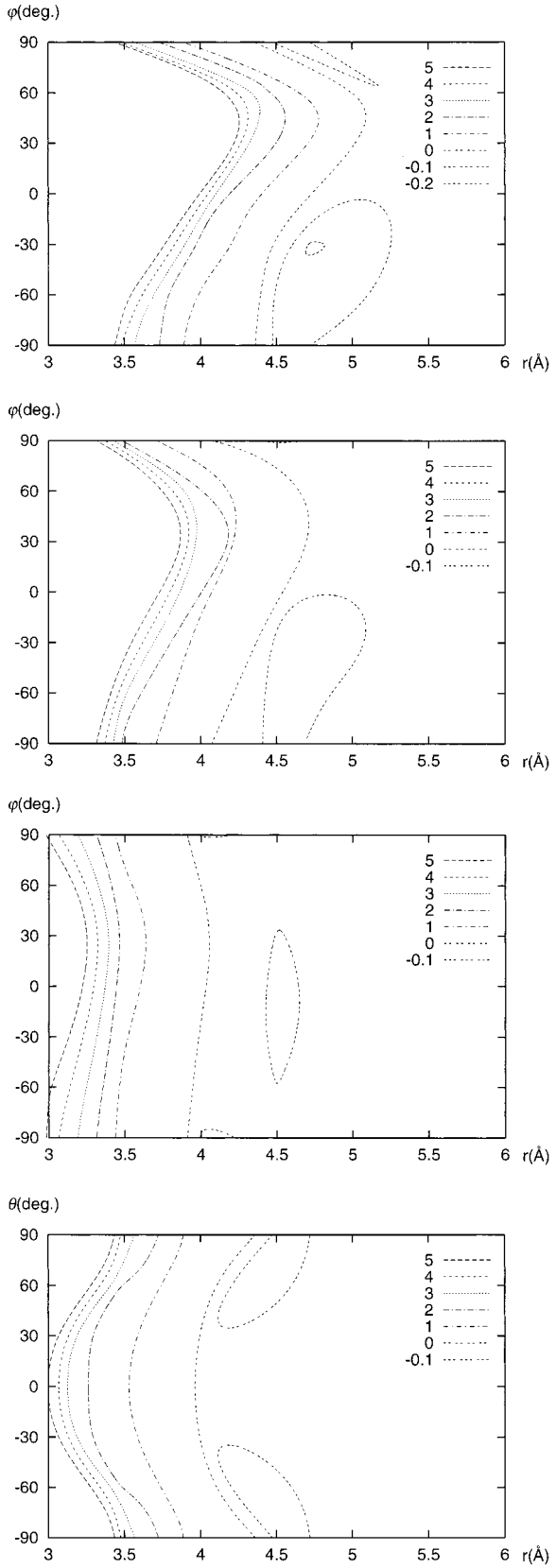

Figure 2. Contour maps of the potential energy surface of S_1 in the glyoxal and Ar system (kcal/mol): (a) cross section of $\theta = 90.0°$, (b) cross section of $\theta = 60.0°$, (c) cross section of $\theta = 30.0°$, and (d) cross section of $\varphi = \pm 90.0°$.

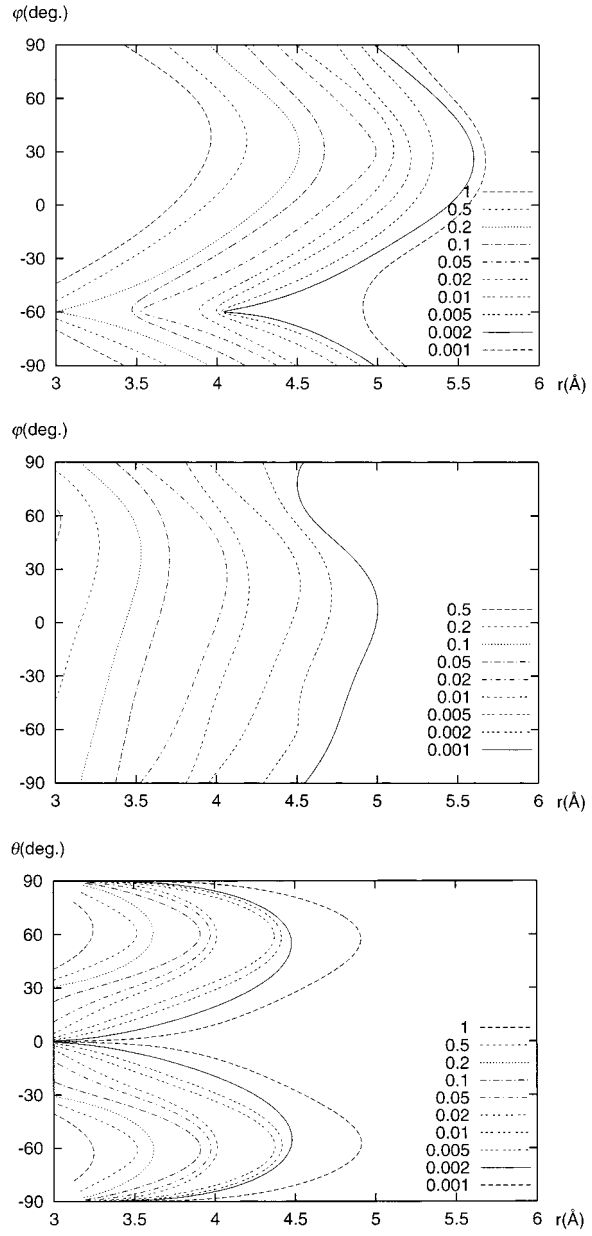

Figure 3. Contour maps of absolute values of matrix elements of the SO interaction between the S_1 and $T_1^{\pm 1}$ states in the glyoxal and Ar system (cm^{-1}): (a) cross section of $\theta = 60.0°$, (b) cross section of $\theta = 30.0°$, and (c) cross section of $\varphi = \pm 90.0°$.

of 5.62−5.98 kcal/mol at the CASSCF level. We shifted the T_1 surface so as to reproduce the S_1-T_1 energy difference by the MRCI method with the Pople correction, 8.24 kcal/mol, at the infinite separation between glyoxal and Ar.

The calculated matrix elements of the intramolecular SO interaction between the S_1 and T_1^0 states of isolated glyoxal are 3.21×10^{-3} cm^{-1} and nearly zero between S_1 and $T_1^{\pm 1}$. The former is consistent to the experimental value suggested by Lombardi et al. (order of 10^{-2} cm^{-1}).[2] Because of the small values of the matrix elements and the Franck−Condon factors, we can easily expect that the intersystem crossing from S_1 to T_1 scarcely occurs in an isolated glyoxal.

The matrix elements of the SO coupling between S_1 and $T_1^{\pm 1}$ in the glyoxal and Ar system are shown in Figure 3a−c, where we used the molecular fixed frame given in Figure 1. Figure 3a−c is drawn on the same cross sections as those in Figure 2b−d, respectively. Note that the absolute value between the S_1 and T_1^{+1} is the same as that between S_1 and T_1^{-1} and the intermolecular SO coupling elements becomes zero when Ar is placed on the $x-y$ plane, the molecular plane of glyoxal. As seen in Figure 3, the SO coupling elements change remarkably depending on the positions of Ar relative to glyoxal, indicating that the intermolecular contribution is important in these elements. On the other hand, the SO element between the S_1 and T_1^0 states is almost constant irrespective of the position of Ar and close to the value of isolated glyoxal. Comparing Figure 3 with Figure 2, we can find that the SO interaction is more sensitive to the position of Ar than the interaction energy and cannot be disregarded even at the region where the interaction energy is sufficiently small. For example, the SO matrix element becomes about 7 times the intramolecular contribution at the point where the van der Waals complex is formed, $r = 4.5$ Å, $\theta = 60.0°$, and $\varphi = \pm 90.0°$, from Figures 2b and 3a. It is also noted that the intermolecular term becomes more than 300 times the intramolecular one in the region where Ar can approach at a room temperature ($r = 3.474$ Å, $\theta = 60.0°$, and $\varphi = \pm 90.0°$). In particular, it becomes very large when Ar is located near the oxygen atom. Thus, the intermolecular one results from the overlap between the 3p orbitals of Ar and the π (π^*) orbitals of the CO moiety of glyoxal. Considering that the intermolecular SO coupling is larger than the intramolecular one and strongly depends on the position of Ar, the collision-induced intersystem crossing seems to be dominated by the intermolecular SO contribution which is induced by the approach of Ar.

We first carried out the dynamics calculations based on method 1, in which the relaxation effect on the T_1 surface is not taken into account. The transition probability from the S_1 to T_1 state was calculated as the function of orientation angle of Ar and orbital angular momentum l. It was found that the transition probability strongly depends on the orientation angles, θ and φ, and l. (2.82×10^{-12} to 1.47×10^{-10} at 100.0 K and 3.17×10^{-12} to 8.58×10^{-10} at 298.15 K, excluding the intermolecular SO interaction; on the other hand, 3.02×10^{-12} to 1.17×10^{-7} at 100.0 K and 3.18×10^{-12} to 4.24×10^{-7} at 298.15 K, including the interaction.) To clarify the effect of the intermolecular SO interaction in the intersystem crossing, we further estimated the cross sections in each approaching orientation of Ar. Without the intermolecular one, the angle-dependent cross sections are in the range of 8.09×10^{-8} ($\theta = 30.0°$, $\varphi = 30.0°$) to 1.66×10^{-7} ($\theta = 90.0°$, $\varphi = -30.0°$) at 100.0 K and 2.25×10^{-7} ($\theta = 90.0°$, $\varphi = 30.0°$) to 1.06×10^{-6} ($\theta = 90.0°$, $\varphi = -30.0°$) at 298.15 K. However, when the intermolecular contribution is included, some of these cross sections dramatically increased, ranging from 9.35×10^{-8} ($\theta = 60.0°$, $\varphi = -60.0°$) to 1.14×10^{-4} ($\theta = 60.0°$, $\varphi = 0.0°$) at 100.0 K and 2.25×10^{-7} ($\theta = 90.0°$, $\varphi = 30.0°$) to 5.68×10^{-4} ($\theta = 60.0°$, $\varphi = 0.0°$) at 298.15 K. In particular, the ratios of the maximum to the minimum among them by only the intramolecular SO interaction are 2.1 at 100.0 K and 4.7 at 298.15 K. On adding the intermolecular one, those become 1213.8 at 100.0 K and 2526.2 at 298.15 K. Moreover, we mention several ratios largely affected by the intermolecular one within the same orientation: 1100.1 ($\theta = 60.0°$, $\varphi = 0.0°$), 765.2 ($\theta = 60.0°$, $\varphi = 30.0°$), and 134.6 ($\theta = 60.0°$, $\varphi = \pm 90.0°$) at 100.0 K; 1246.7 ($\theta = 60.0°$, $\varphi = 30.0°$), 1206.0 ($\theta = 60.0°$, $\varphi = 0.0°$), and 354.0 ($\theta = 60.0°$, $\varphi = \pm 90.0°$) at 298.15 K. These show that the orientation dependence is extremely strong in this intersystem crossing due to the unevenly distributed intermolecular SO interaction. The present results seem to support the suggestion by Dai and co-workers[5] that the magnitude of the SO interaction depends on the orientation of Ar relative to glyoxal and the lifetime of S_1 fluctuates

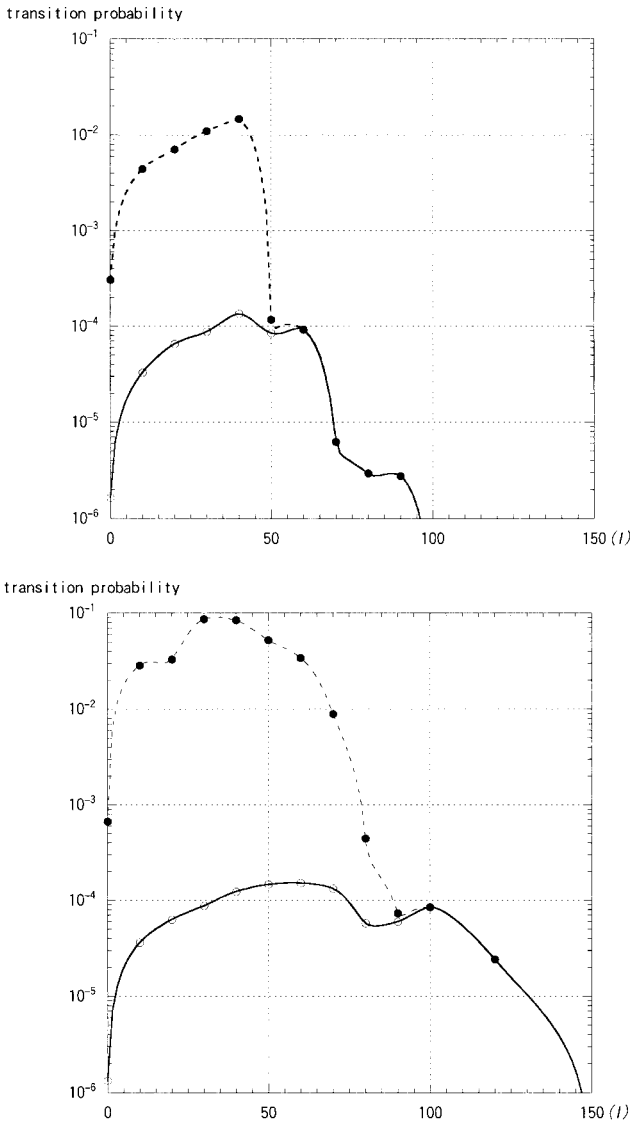

Figure 4. Transition probabilities obtained by method 2 as a function of orbital angular momentum quantum number l: (a) at 100.0 and (b) 298.15 K. These values are averaged with respect to the orientations and weighted by the number of rotational states $2l + 1$.

significantly depending on the conformations of glyoxal−Ar van der Waals complexes.

Next, we examined the relaxation effect on the transition by applying method 2. The transition probabilities as the functions of l are shown in Figure 4, in which these are averaged with respect to the orientations and weighted by $2l + 1$. In the small l region, the transition probability including the intermolecular term become more than a few hundreds times at 100.0 K (Figure 4a) and 298.15 K (Figure 4b) of those excluding it. As showed in Figure 4, the contribution from the intermolecular one becomes small in the region of $l > 50$ at 100.0 K and $l > 90$ at 298.15 K, the impact parameters of 2.94 and 5.28 Å, respectively. The angle-dependent cross sections are in the range of 1.61×10^{-3} ($\theta = 90.0°$, $\varphi = 30.0°$) to 1.16×10^{-2} ($\theta = 90.0°$, $\varphi = 60.0°$) at 100.0 K and 7.20×10^{-3} ($\theta = 90.0°$, $\varphi = -60.0°$) to 1.97×10^{-2} ($\theta = 90.0°$, $\varphi = 0.0°$) at 298.15 K, including only the intramolecular SO coupling. They are enhanced by including the intermolecular contribution, in the range of 1.62×10^{-3} ($\theta = 90.0°$, $\varphi = 30.0°$) to $3.10 \times 10°$ ($\theta = 60.0°$, $\varphi = \pm 90.0°$) at 100.0 K and 7.20×10^{-3} ($\theta = 90.0°$, $\varphi = -60.0°$) to 2.42×10^{1} ($\theta = 60.0°$, $\varphi = 0.0°$) at 298.15 K.

TABLE 4: Total Cross Sections of Intersystem Crossing from S_1 to T_1 in Glyoxal (Å^2)[a]

	intramolecular spin−orbit coupling		intra- and intermolecular spin−orbit coupling	
	100.0 K	298.15 K	100.0 K	298.15 K
method 1	1.17×10^{-7}	5.18×10^{-7}	1.23×10^{-5}	7.59×10^{-5}
	(3.10×10^{-19})	(2.37×10^{-18})	(3.26×10^{-17})	(3.47×10^{-16})
method 2	4.41×10^{-3}	1.41×10^{-2}	2.42×10^{-1}	2.65×10^{0}
	(1.17×10^{-14})	(6.45×10^{-14})	(6.42×10^{-13})	(1.21×10^{-11})

[a] Transition rate constants are also presented in parenthese (cm^3 s^{-1}). Observed quenching rate constant and cross section are 1.8×10^{-11} cm^3 s^{-1} and 3.5 Å^2, which are taken from ref 1b.

As with the case of method 1, the calculated ratios of the maximum to the minimum are 7.2 at 100.0 K and 2.7 at 298.15 K without the intermolecular SO interaction and, on the other hand, 1918.4 at 100.0 K and 3361.4 at 298.15 K with that. The large cross sections ratios in the same orientation angle are 456.8 ($\theta = 60.0°$, $\varphi = \pm 90.0°$), 227.2 ($\theta = 60.0°$, $\varphi = 0.0°$), and 152.9 ($\theta = 60.0°$, $\varphi = 30.0°$) at 100.0 K and 1844.5 ($\theta = 60.0°$, $\varphi = 0.0°$), 1743.2 ($\theta = 60.0°$, $\varphi = 30.0°$), 300.8 ($\theta = 60.0°$, $\varphi = \pm 90.0°$), and 245.3 ($\theta = 60.0°$, $\varphi = 60.0°$) at 298.15 K. Compared to the results by method 1, the relaxation effect increases the intersystem crossing probability by the intermolecular one, especially in the case at 298.15 K.

The IOS approximation has been frequently used in the calculation of collision dynamics. However, Billing and Clary investigated the collisions of polyatomic molecules with atoms and found out that the IOS approximation tends to be less accurate for heavy mass systems.[23] In the present study, the simple semiclassical dynamics method based on the IOS approximation was used to deal with the collision-induced vibrational−rotational relaxations by introducing the level widths of the vibrational states of T_1 and to estimate the effect of the intermolecular SO interaction roughly. For the qualitative and quantitative improvement, it is desirable to adopt the semiclassical models developed to describe energy transfer in polyatomic molecules.[24]

The calculated total cross sections and transition rate constants are summarized in Table 4. With method 1, the calculated cross sections are quite small. The ratios between the cross sections with and without the intermolecular SO interaction are 105.1 at 100.0 K and 146.5 at 298.15 K. On the other hand, the total cross sections become considerably large taking account of the relaxation effect by method 2. The calculated total cross section (2.65 Å^2 at 298.15 K) is comparable to the experimental value (3.5 Å^2 at 300.0 K). The total cross section is enhanced by 54.9 times at 100.0 K and 187.9 at 298.15 K due to the intermolecular SO contribution. Although the intermolecular SO interaction is local, it is extremely strong compared with the intramolecular one. Thus, the effect of the intermolecular one remains remarkable even after averaging over whole orientations. However, these total cross sections by method 2 are remarkably sensitive to the level width. For instance, the total cross sections with the level width of 0.1 cm^{-1} are 1100−1400 times smaller than those with the level width of 1.0 cm^{-1}.

Freed et al.[4] asserted the importance of the relaxation processes, especially the rotational relaxation, in the collision-induced intersystem crossing. We make sure of their arguments about the relaxation effect through the present dynamical calculations. Furthermore, our results show that the intermolecular SO interaction is also an important factor in this system.

4. Conclusion

We have theoretically studied the intersystem crossing from the S_1 state of glyoxal induced by the collision of Ar. The interaction potentials of S_1 and T_1 and the SO interaction between these states in the glyoxal and Ar system were calculated by using ab initio MO method. The semiclassical dynamics calculations were also carried out in order to estimate the transition cross sections and rate constants.

From the potential energy surface of S_1, the existence of van der Waals complexes is confirmed in the regions partially corresponding to those suggested by Dai and co-workers.[5] Although the magnitude of the SO interaction is very small, it depends heavily on the orientations of Ar relative to glyoxal. In particular, the SO interaction is remarkably induced by the approach of Ar from out of the glyoxal molecular plane since the intermolecular part is caused by the interaction between the π (π^*) orbitals of glyoxal and the valence orbitals of Ar. The dynamics calculations reveal that the intermolecular SO interaction increases the transition cross section more than 100 times the value by only the intramolecular one at 298.15 K even if the total cross sections are obtained by averaging over whole orientations. Further, it is also found that the relaxation processes (vibrational and rotational relaxations) are indispensable to dealing with this collision-induced intersystem crossing from S_1 to T_1.

We recognize two problems in the present study, namely, the instability problem in the electronic state calculations for the excited states of glyoxal and the treatment for relaxation in the dynamics calculation. The instability problem mainly affects the normal-mode frequencies in glyoxal and the interactions between glyoxal and Ar, e.g., the interaction potentials and the SO interaction. Although the effect to the interactions is avoided by the use of the fixed structure of C_{2h} for glyoxal and the first-order convergence procedure in the CASSCF method, the vibrational modes with high frequencies do not correspond with those in the experiments. To solve the instability problem proficiently, it is necessary to employ the method including the dynamic electron correlation in the geometry optimizations and normal-mode analyses.

It is often pointed out that the vibrational−rotational relaxation must be considered in the electronic transition. In the present study, the calculated total cross sections without the relaxation effect are far from those by the experiments. The value becomes comparable to the experimental one by introducing a parameter for lifetime of vibrational states as the relaxation effect in the T_1 state. However, the technique to deal with relaxation processes in dynamics calculations must be developed further to research electronic transitions in chemical systems.

Acknowledgment. We thank Prof. K. Hirao for his valuable advice on the electronic structure theory. We are also grateful to Dr. H. Sato and Prof. K. Yamashita for their fruitful discussions and encouragement. Numerical calculations were carried out at IMS Computer Center. This work was supported by the Grant in Aid for Scientific Research from the Ministry of Education.

References and Notes

(1) (a) Beyer, R. A.; Zittel, P. F.; Lineberger, W. C. *J. Chem. Phys.* **1975**, *62*, 4016. (b) Beyer, R. A.; Lineberger, W. C. *J. Chem. Phys.* **1975**, *62*, 4024. (c) Zittel, P. F.; Lineberger, W. C. *J. Chem. Phys.* **1977**, *66*, 2972.

(2) (a) Lombardi, M.; Jost, R.; Michel, C.; Tramer, A. *Chem. Phys.* **1980**, *46*, 273. (b) Lombardi, M.; Jost, R.; Michel, C.; Tramer, A. *Chem. Phys.* **1981**, *57*, 341. (c) Lombardi, M.; Jost, R.; Michel, C.; Tramer, A. *Chem. Phys.* **1981**, *57*, 355. (d) Dupre, P.; Jost, R.; Lombardi, M. *Chem. Phys.* **1984**, *91*, 355. (e) Michel, C.; Lombardi, M.; Jost, R. *Chem. Phys.* **1986**, *109*, 357.

(3) Holtzclaw, K. W.; Moss, D. B.; Parmenter, C. P.; Loge, G. W. *J. Phys. Chem.* **1983**, *87*, 4495.

(4) (a) Freed, K. F.; *Adv. Chem. Phys.* **1980**, *42*, 207. (b) Freed, K. F. *Adv. Phys. Chem.* **1981**, *47-II*, 291. (c) Gelbart, W. M.; Freed, K. F. *Chem. Phys. Lett.* **1973**, *18*, 470. (d) Freed, K. F. *Chem. Phys. Lett.* **1976**, *37*, 47. (e) Freed, K. F. *J. Chem. Phys.* **1976**, *64*, 1604.

(5) (a) Lapierre, L.; Dai, H. L. *J. Chem. Phys.* **1992**, *97*, 711. (b) Lapierre, L.; Frye, D.; Dai, H. L. *J. Chem. Phys.* **1991**, *96*, 2703.

(6) Hoffmann, M. R.; Schatz G. C. *J. Chem. Phys.* **2000**, *113*, 9456.

(7) Dunning, T. H. *J. Chem. Phys.* **1970**, *53*, 2823.

(8) Mclean, A. D.; Chandler, G. S. *J. Chem. Phys.* **1980**, 72, 5639.

(9) Dupuis, M.; Chin, S.; Marquez, A. In *CHEM-Station And HONDO in Relativistic and Electron Correlation Effects in Molecular and Clusters*; Malli, G. L., Ed.; Plenum: New York, 1992.

(10) Frisch, M. J.; Trucks, G. W.; Schlegel, H. B.; Gill, P. M.; Johnson, B. G.; Robb, M. A.; Cheeseman, J. R.; Keith, T. A.; Petersson, G. A.; Montgomery, J. A.; Raghavachari, K.; Al-Laham, M. A.; Zakrzewski, V. G.; Ortiz, J. V.; Foresman, J. B.; Cioslowski, J.; Stefanov, B. B.; Nanayakkara, A.; Challacombe, M.; Peng, C. Y.; Ayala, P. Y.; Chen, W.; Wong, M. W.; Andres, J. L.; Replogle, E. S.; Gomperts, R.; Martin, R. L.; Fox, D. J.; Binkley, J. S.; Defrees, D. J.; Baker, J.; Stewart, J. P.; Head-Gordon, M.; Gonzalez, C.; Pople, J. A. *Gaussian 94*; Gaussian, Inc.: Pittsburgh, PA, 1995.

(11) (a) Kupka, H.; Cribb, P. H. *J. Chem. Phys.* **1986**, *85*, 1303. (b) Hougen, J. T.; Watson, J. K. G. *Can. J. Phys.* **1965**, *43*, 298. (c) Sharp, T. E.; Rosenstock, H. M. *J. Chem. Phys.* **1964**, *41*, 3453. (d) Lucas, N. J. D. *J. Phys. B* **1973**, *6*, 155.

(12) Werner, H.-J.; Knowles P. J.; with contributions from Almlöf, J.; Amos, R. D.; Deegan, M. J. O.; Elbert, S. T.; Hampel, C.; Meyer, W.; Peterson, K.; Pitzer, R.; Stone, A. J.; Taylor, P. R.; Lindh, R. *MOLPRO*; University of Birmingham: Birmingham, U.K., 1996.

(13) (a) Langhoff, S. R.; Davidson, E. R. *Int. J. Quantum Chem.* **1974**, *8*, 61. (b) Del Bene, J. E.; Shavitt, I. *Int. J. Quantum Chem. Quantum Chem. Symp.* **1989**, *445*. (c) van de Bovenkamp, J.; van Mourik, T.; van Duijneveldt, F. B. *Mol. Phys.* **1999**, *97*, 487.

(14) Knowles, P. J.; Handy, N. C. *Chem. Phys. Lett.* **1984**, *111*, 315.

(15) Murrell, J. N.; Carter, S.; Farantos, S. C.; Huxley, P.; Varandas, A. J. C. *Molecular Potential Energy Functions*; John Wiley and Sons: New York, 1984.

(16) (a) Breit, G. *Phys. Rev.* **1929**, *34*, 553. (b) Langhoff, S. R. In *Modern Theoretical Chemistry*; Schaefer, H. F., Ed.; Plenum: New York, 1977; Chapter 10.

(17) King, H. F.; Furlani, T. R. *J. Comput. Chem.* **1988**, *9*, 771.

(18) Child, M. S. *Molecular Collision Theory*; Academic Press: London, 1974.

(19) Kouri, D. J. In *Atom-Molecular Collision Theory*; Bernstein, R. B., Ed.,; Plenum: New York, 1979; Chapter 7.

(20) (a) Freed, K. F.; Jortner, J. *J. Chem. Phys.* **1969**, *50*, 2916. (b) Freed, K. F. *J. Chem. Phys.* **1970**, *52*, 1345. (c) Bixon, M.; Dothan, Y.; Jortner, J. *Mol. Phys.* **1969**, *17*, 109.

(21) (a) Nitzsche, L. E.; Davidson, E. R. *Chem. Phys. Lett.* **1978**, *58*, 171. (b) Hirao, K. *J. Chem. Phys.* **1983**, *79*, 5000. (c) Engelbrecht, L.; Liu, B. *J. Chem. Phys.* **1983**, *78*, 3097.

(22) (a) Birss, F. W.; Brown, J. M.; Core, A. R. H.; Lofthus, A.; Krishnamachari, S. L. N. G.; Osborne, G. A.; Paldus, J.; Ramsay, D. A.; Watmann, L. *Can. J. Phys.* **1970**, *48*, 1230. (b) Holzer, W.; Ramsay, D. A. *Can. J. Phys.* **1970**, *48*, 1759. (c) Goetz, W.; Mchugh, A. J.; Ramsay, D. A. *Can. J. Phys.* **1970**, *48*, 1. (d) Paldus, J.; Ramsay, D. A. *Can. J. Phys.* **1967**, *45*, 1389. (e) Brand, J. C. D. *Trans. Faraday Soc.* **1954**, *50*, 431. (f) Dong, R. Y.; Names, R.; Ramsay, D. A. *Can. J. Chem.* **1993**, *71*, 1595. (g) Ottinger, Ch.; Winkler, T. *Chem. Phys. Lett.* **1999**, *314*, 411. (h) Stanton, J. F.; Gauss, J. *Spectrochim. Acta, Part A* **1997**, *53*, 1153. (i) Briss, F. W.; Braund, D. B.; Cole, A. R. H.; Engleman, R.; Green, A. A.; Japar, S. M.; Nanes, R.; Orr, B. J.; Ramsay, D. A.; Szyszka, J. *Can. J. Phys.* **1971**, *49*, 317. (j) Kuchitsu, K.; Fukuyama, T.; Morino, Y. *J. Mol. Struct.* **1969**, *4*, 41.

(23) Billing, G. D.; Clary, D. C. *Chem. Phys. Lett.* **1982**, *90*, 27.

(24) (a) Billing, G. D. *Chem. Phys.* **1993**, *173*, 167. (b) Billing, G. D.; Clary, D. C. *Chem. Phys.* **1983**, *80*, 213. (c) Billing, G. D. *Chem. Phys.* **1983**, *76*, 315.